Hindawi
Journal of Chemistry
Volume 2017, Article ID 7943164, 11 pages
https://doi.org/10.1155/2017/7943164

Research Article

Preparation of $CoFe_2O_4/SiO_2$ Nanocomposites at Low Temperatures Using Short Chain Diols

Thomas Dippong,[1] Erika Andrea Levei,[2] and Oana Cadar[2]

[1]*Department of Chemistry and Biology, Technical University of Cluj-Napoca, North University Centre of Baia Mare, 76 Victoriei Street, 430122 Baia Mare, Romania*
[2]*INCDO-INOE 2000, Research Institute for Analytical Instrumentation, 67 Donath Street, 400293 Cluj-Napoca, Romania*

Correspondence should be addressed to Erika Andrea Levei; erika.levei@icia.ro

Received 2 January 2017; Accepted 31 January 2017; Published 15 March 2017

Academic Editor: Jean-Marie Nedelec

The preparation of 70% $CoFe_2O_4$/30% SiO_2 (wt%) nanocomposites by sol-gel method using three short chain diols (1,2-ethanediol, 1,3-propanediol, and 1,4-butanediol) as chelators was studied. The Fourier transformed infrared spectra and X-ray diffraction patterns were used to confirm the formation of nanocomposites. The X-ray diffraction analysis showed that the chain length of the carboxylates embedded in the silica matrix influences the formation of crystallized cobalt ferrite as single phase at low temperatures. The influence of the methylene groups number in the precursors and annealing temperature on the nanocrystallite size was revealed. The stability of the obtained compounds was determined by calculation of thermodynamic parameters.

1. Introduction

During the last decades, the nanocomposites preparation techniques experienced a fast development as these materials have a wide range of applications [1–4]. The properties of nanoparticle-based composites are determined by the material's morphology, which depends on the nanoparticle size and distribution of the nanosized phase in matrix [5]. Cobalt ferrite based nanocomposites present unique physicochemical properties that make it an attractive material for catalysis, antenna rods, loading coils, magnetic data storage, sensors, ferrofluids, magnetooptic materials, energy conversion applications, and targeted drug delivery [1–6].

The preparation methods for $CoFe_2O_4$ nanoparticles require special techniques to prevent agglomeration [7, 8]. A high number of methods have been reported previously for the preparation of $CoFe_2O_4$ nanoparticles, including microemulsion, thermal decomposition, reverse micelles, coprecipitation, sol-gel, mechanical alloying, combustion, and hydrothermal, electrochemical procedures, and green synthesis [9–18]. However, the sol-gel technique followed by annealing is one of the simplest, most effective, and feasible routes to produce high purity, homogeneous, and crystalline nanoparticles [19–21].

In the present study, the influence of the chelator chain length (1,2-ethanediol (1,2-ED), 1,3-propanediol (1,3-PD), and 1,4-butanediol (1,4-BD)) on the precursor formation and decomposition to obtain 70% $CoFe_2O_4$/30% SiO_2 (wt%) nanocomposites was investigated. The obtained gels were heated to 300°C, annealed at 500, 700, and 900°C, and characterized by thermal analysis (TG and DTA), X-ray diffraction (XRD), Fourier transformed infrared spectrometry (FT-IR), scanning electron microscopy (SEM), and transmission electron microscopy (TEM).

2. Materials and Methods

2.1. Synthesis. The used reagents were $Fe(NO_3)_3{\cdot}9H_2O$ as iron source, $Co(NO_3)_2{\cdot}6H_2O$ as cobalt source, 1,2-ED, 1,3-PD, and 1,4-BD as chelators, tetraethyl orthosilicate (TEOS) as matrix precursor, ethanol as solvent, and HNO_3. All reagents were of analytical grade and used as received without further purification.

The sol was prepared by dissolving $Fe(NO_3)_3{\cdot}9H_2O$ and $Co(NO_3)_2{\cdot}6H_2O$ in molar ratio of 2 : 1 and the diol (NO_3^- : diol = 1 : 1, molar ratio), at room temperature, in ethanol/HNO_3 solution. An amount of TEOS equal to 70% of the weight of Fe(III) and Co(II) nitrates was added dropwise under continuous stirring, followed by the addition of ethanol until complete dispersion. The resulting clear solution was exposed to open air for slow gelation. The gelation time was 16 days (1,2-ED), 19 days (1,3-PD), and 23 days (1,4-BD), respectively. The gels were heated at 300°C for 4 hours and afterwards annealed at 500, 700, and 900°C.

The redox reaction between the nitrates and diol (1,2-ED, 1,3-PD, and 1,4-BD) with formation of the carboxylate precursors takes place according to (1).

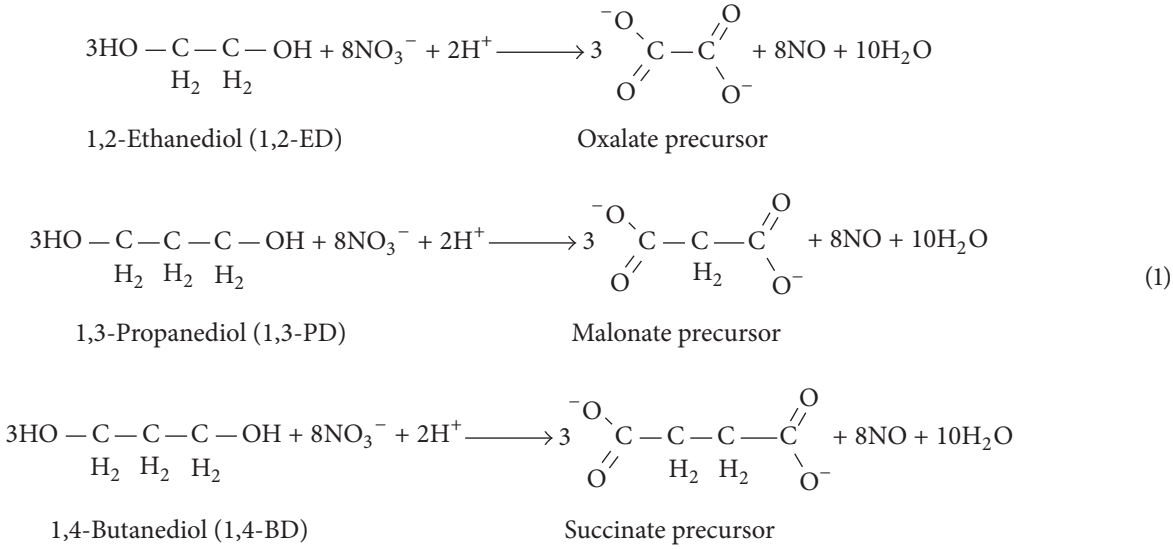

(1)

2.2. Characterization. FT-IR spectra were recorded in transmission mode on KBr pellets using a Perkin-Elmer Spectrum BX II FT-IR spectrometer. XRD analysis was performed at room temperature, using a Bruker D8 Advance diffractometer using a CuK_α radiation (λ = 1.54060 Å). Thermogravimetry (TG) and Differential Thermal Analyses (DTA) were performed by a SDT Q600 type instrument from the room temperature up to 900°C, with a rate of heating of 10°C/min, in air. For the nanocrystallites' shape and clustering, a Hitachi HD-2700 TEM equipped with digital image recording system and photographic film image with high resolution scanner was used with samples deposited from suspension onto carbon film on 400 mesh copper grids. The SEM measurements were carried out using a Hitachi SU-8230 ultrahigh resolution scanning electron microscope and the samples were sputter-coated with 5 nm gold.

3. Results and Discussion

3.1. FT-IR and XRD Analysis. The FT-IR spectra (Figure 1) for the gels dried at 40°C show the presence of nitrates characterized by an intense band at 1384 cm^{-1}, indicating that the redox reaction was not initiated at this temperature. In contrast, the absence of this band in gels dried at 140°C suggests the consumption of nitrates in the redox reaction with formation of the carboxylates [22–24].

The FT-IR spectra of gels dried at both 40 and 140°C show the characteristic bands for the silica matrix: the vibration of Si-O bond at 480 cm^{-1}, the vibration of SiO_4 tetrahedra at 800 cm^{-1}, and the stretching vibration of Si-O-Si bonds at 1063 cm^{-1} [11, 25–27]. The broad band at 3400–3500 cm^{-1} was assigned to the vibration of OH groups in water and silica matrix. The vibration bands of bonded Si-OH expected at 3200–3400 cm^{-1} overlap the broad band of water. In the range of 2900–3000 cm^{-1}, the characteristic bands for C-H bonds of the methylene groups (CH_2) were observed [28–30]. In all FT-IR spectra, a characteristic band for M-O (M = Fe, Co) vibrations appears at 446 cm^{-1}. Moreover, the M-OH groups on the surface of the ferrite particles are replaced by M-O-SiO_3 [31]. In case of gels dried at 40°C, the sharp bands at 1650 cm^{-1} are attributable to the deformation vibration of the H-O-H bond, which indicates the presence of water incorporated in the silica matrix [28, 29]. By increasing the temperature to 140°C, the characteristic bands for the carboxylate type ligands at 1617 cm^{-1} and 1360 cm^{-1} attributed to asymmetric and symmetric vibration of the COO^- groups increase, while characteristic bands for the nitrate decrease in intensity. These results are confirmed by the thermal analysis that indicated the decomposition of nitrates at 80–140°C. The small peak at 1069 cm^{-1} was assigned to the C-O stretching, while those from 1000–700 cm^{-1} were assigned to the C-OH group trapped in the matrix [31]. In case of gels dried at 140°C, the intensity of the bands decreases from oxalate to succinate, probably due to the removal of the two carboxylate groups. The characteristic bands of carboxylates may overlap the bands of the silica matrix [22].

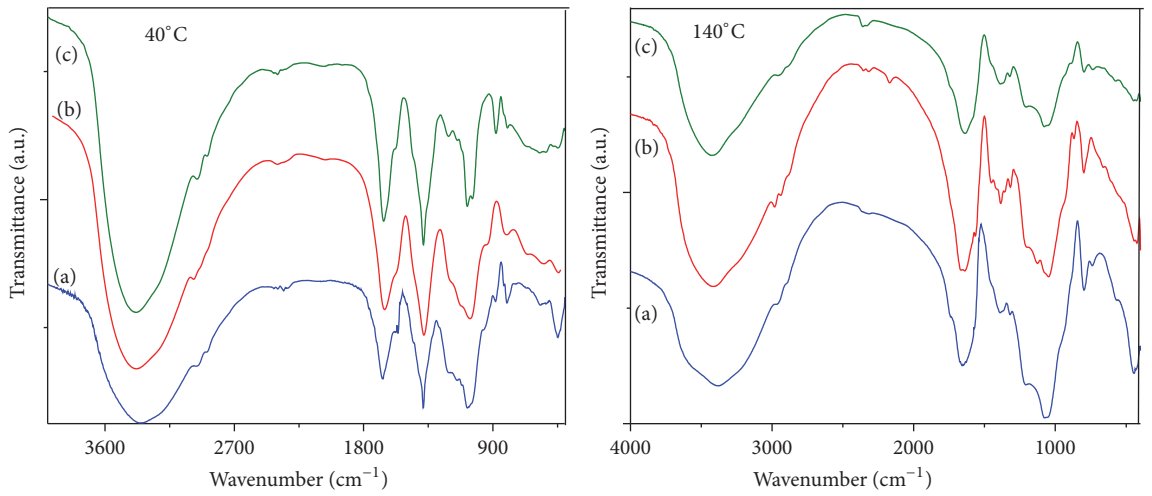

FIGURE 1: FT-IR spectra of the gels obtained using 1,2-ED (a), 1,3-PD (b), and 1,4-BD (c) dried at 40°C and 140°C.

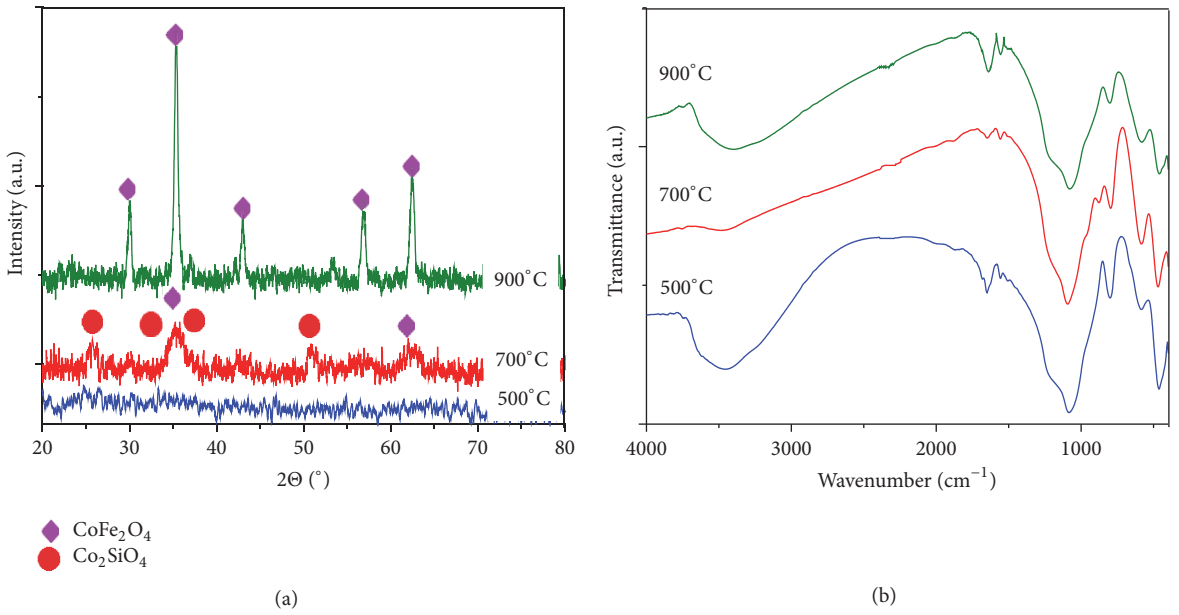

FIGURE 2: XRD patterns (a) and FT-IR spectra (b) of the gels obtained using 1,2-ED, annealed at 500, 700, and 900°C.

Figures 2–4 present the XRD patterns (a) and FT-IR spectra (b) of the gels obtained using 1,2-ED, 1,3-PD, and 1,4-BD, respectively, annealed at 500, 700, and 900°C. The diffraction pattern of gels obtained using 1,2-ED (Figure 2(a)) annealed at 500°C did not show the presence of crystalline phase, while the FT-IR spectrum (Figure 2(b)) showed both the characteristic bands for the silica matrix (Si-O bonds vibration at 480 cm^{-1}; SiO_4 tetrahedron vibration at 798 cm^{-1} and Si-O-Si bonds stretching vibration at 1080 cm^{-1}; H-OH bond deformation vibration at 1650 cm^{-1}; vibration of OH groups in water and silica matrix at 3400–3500 cm^{-1}) and the characteristic bands for the M-O bond at 400–500 cm^{-1} [11, 25, 26, 31] which indicates the formation of cobalt ferrite, insufficiently crystallized to be noticed in the XRD pattern. At 700°C, the XRD patterns show the formation of poorly crystallized cobalt ferrite (JCPDS File number 42-1467) contaminated with olivine type cobalt silicate (Co_2SiO_4) (JCPDS File number 87-0053). The formation of olivine at 700°C could be explained by the experimental set-up that inhibits the formation of Co_3O_4 spinel oxide up to 900°C and favors the formation of CoO at lower temperatures. The formed CoO reacts with the amorphous SiO_2 during annealing and forms olivine [22]. The FT-IR spectrum of the gel annealed at 700°C shows, in addition to the characteristic

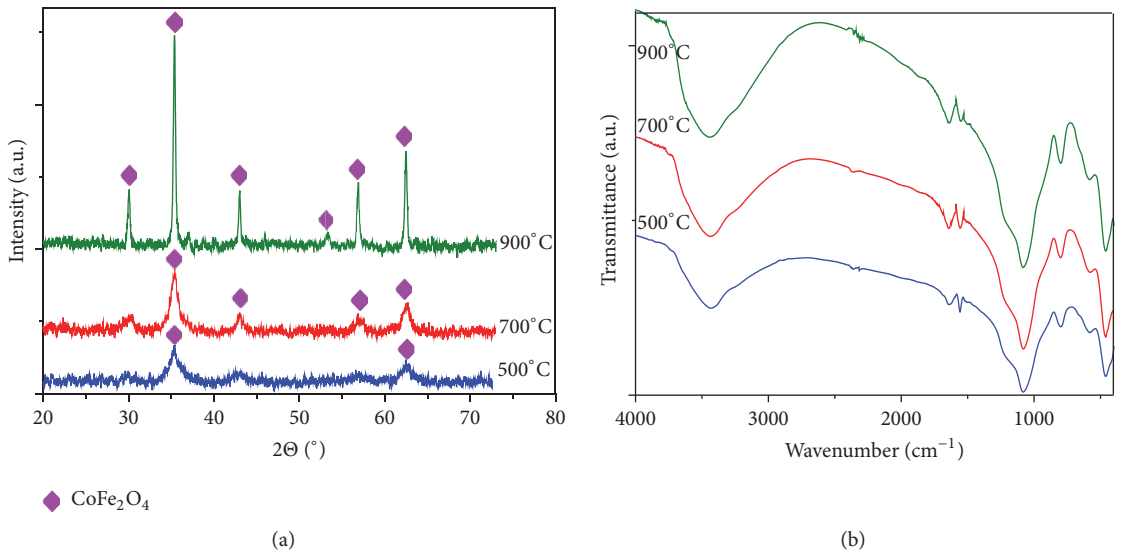

Figure 3: XRD patterns (a) and FT-IR spectra (b) of the gels obtained using 1,3-PD, annealed at 500, 700, and 900°C.

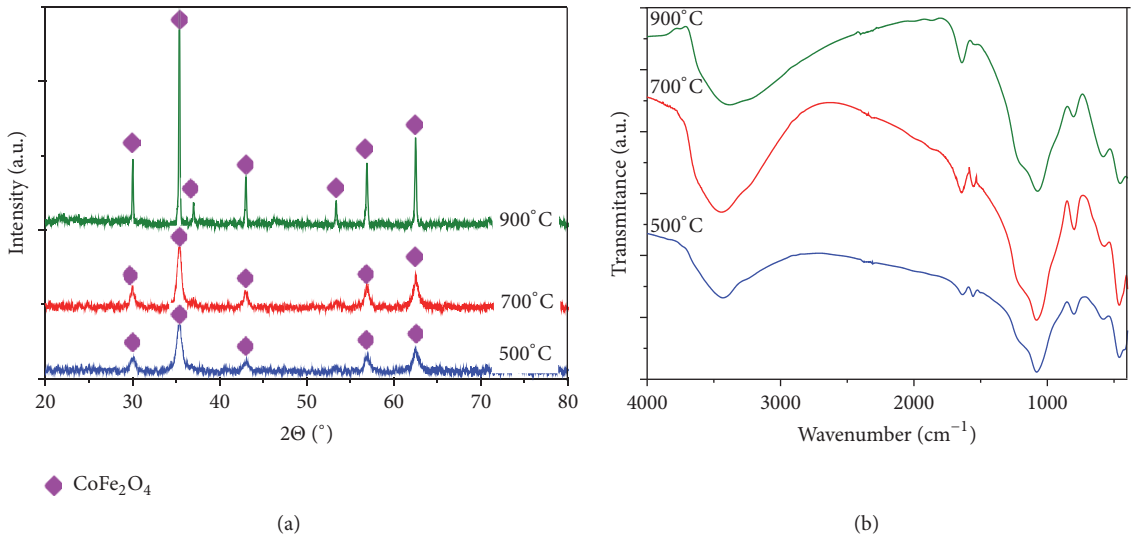

Figure 4: XRD patterns (a) and FT-IR spectra (b) of the gels obtained using 1,4-BD, annealed at 500, 700, and 900°C.

bands of the silica matrix, the characteristic bands for cobalt silicate (571 and 870 cm^{-1}) [25, 26, 32, 33]. The formation of well crystallized single phase $CoFe_2O_4$ spinel in the silica matrix occurs at 900°C. This can be explained by the fact that the reaction between CoO (formed from Co_3O_4) and Fe_2O_3 is more thermodynamically favored than the reaction between CoO and SiO_2 [22]. The FT-IR spectrum shows the characteristic bands for $CoFe_2O_4$ (466 and 594 cm^{-1}) and the bands of silica matrix, which are more intense than in the previous cases.

The XRD patterns of the gels obtained using 1,3-PD (Figure 3(a)) show the development of crystalline $CoFe_2O_4$ (JCPDS File number 42-1467). By annealing at 500°C, poorly crystallized $CoFe_2O_4$ is formed. By increasing the annealing temperature to 700 and 900°C, the degree of crystallization increases. At 700°C, the cobalt ferrite formation is more thermodynamically favored than the formation of olivine. The FT-IR spectra (Figure 3(b)) show characteristic bands for $CoFe_2O_4$ (466 and 594 cm^{-1}) and silica matrix (480, 798, 1080, 1650, and 3400–3500 cm^{-1}) [25, 26, 31, 32].

At all annealing temperatures, the XRD pattern of gels obtained from 1,4-BD (Figure 4(a)) shows the formation of crystalline $CoFe_2O_4$ as a single phase (JCPDS File number 42-1467). Compared to synthesis using other diols, the

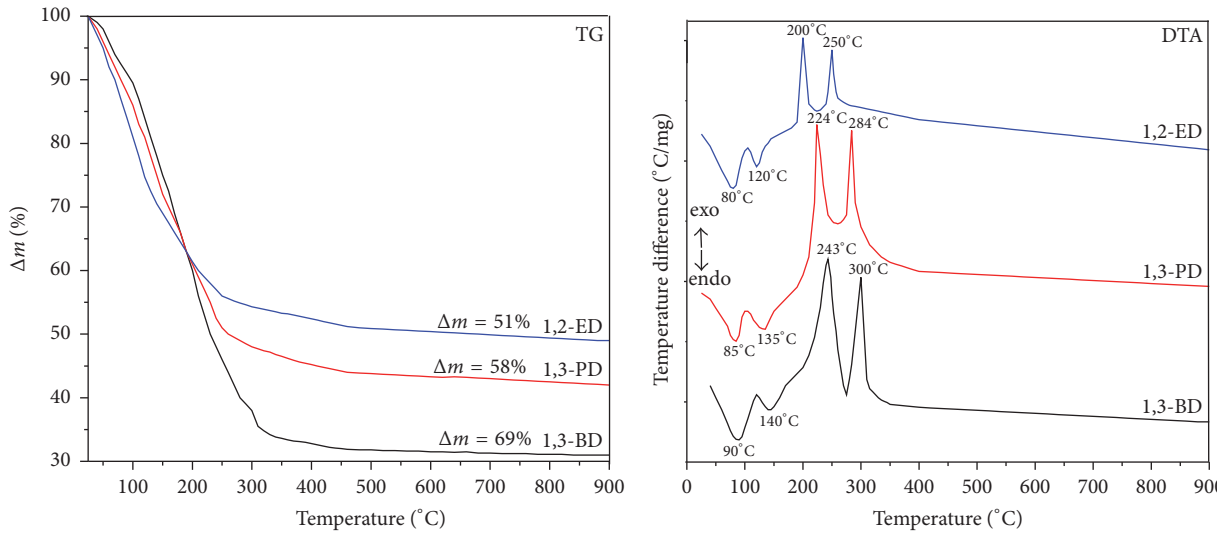

Figure 5: Thermal analysis (TG and DTA) of carboxylate precursors.

Table 1: Average diameters of $CoFe_2O_4$ crystallites calculated according to the Scherrer equation.

Temperature (°C)	Average size (nm)		
	1,2-ED	1,3-PD	1,4-BD
500	—	2	5
700	3	5	11
900	11	15	22

synthesis method using 1,4-BD is very attractive, since it allows the obtaining of $CoFe_2O_4$ spinel at low temperature. In the FT-IR spectra (Figure 4(b)), the specific bands for $CoFe_2O_4$ (466 and 594 cm^{-1}) and silica matrix (480, 798, 1080, 1650, and 3400–3500 cm^{-1}) are present [11, 25, 26, 32].

Based on the XRD patterns and FT-IR spectra it can be concluded that the longer chain length of the carboxylate embedded in the silica matrix favors the formation of crystallized ferrite cobalt single phase at low temperatures. The average size of $CoFe_2O_4$ crystallites was estimated based on the XRD data, using the following Scherrer equation [34]:

$$D = \frac{0.9\lambda}{\beta \cos\theta}, \quad (2)$$

where D is the average crystallite size, λ is the X-ray wavelength, β is the broadening of full width at half maximum (FWHM) intensity of the main intense peak, and θ is Bragg angle.

The average crystallite size (Table 1) indicates that the cobalt ferrite was obtained as nanoparticles. The nanocrystallites sizes increase with the number of methylene groups.

3.2. Thermal Analysis. The formation and decomposition of carboxylate precursors were investigated by the thermal analysis of gels dried at 40°C.

On TG diagram (Figure 5), the weight losses were 51% for 1,2-ED, 58% for 1,3-PD, and 69% for 1,4-BD, respectively, increasing with the increase of the carboxylate precursor chain length, as a consequence of the additional loss of a methylene or ethylene group in the case of malonic and succinic precursors. After 300°C, the mass slowly decreases up to 900°C due to the dehydroxylation of the silica matrix. In all cases, the DTA diagram (Figure 5) shows (i) two endothermic effects corresponding to the redox reaction between nitrates and diol with the formation of carboxylate anions that coordinate to the metallic ions and (ii) two exothermic effects corresponding to the oxidative decomposition of the precursor (oxalate, malonate, and succinate) and the combustion of organic chains intercalated in the silica network. The two exothermic effects at 80–140°C suggest that Fe(III) and Co(II) nitrates react separately with the diol due to the difference of the aqua cations acidity: $pK_{a[Fe(NO_3)_3]}$ = 2.22 and $pK_{a[Co(NO_3)_2]}$ = 12.2 [22, 23]. Thermal behavior of the metal nitrates, diol solutions, suggests the formation of a homogeneous mixture of homonuclear Fe(III) and Co(II) carboxylates. The two endothermic effects at 200–300°C on DTA curves of gels show that the decomposition of precursors takes place in two stages indicating that both Fe(III) and Co(II) carboxylic compounds are formed separately. Thus, the first exothermic effect corresponds to decomposition of cobalt oxalates (200°C), malonates (224°C), and succinates (243°C), while the second exothermic effect corresponds to the decomposition of iron oxalates (250°C), malonates (284°C), and succinates (300°C). The decomposition of gel obtained from 1,4-BD occurs at the highest temperatures, indicating that, by increasing the number of methylene groups, the thermic effect increases and shifts toward higher temperatures.

Table 2: Thermodynamic parameters of the compounds formed during synthesis.

Compound	ΔH^o (kcal/mol)	S^o (cal/mol K)	$c_p{}^o$		
			a	$b \cdot 10^3$	$c \cdot 10^{-5}$
CoO	−56923	12.7	10.8	2.6	14.4
Fe_2O_3	−63200	14.1	12.6	8.5	−0.8
SiO_2	−205	10.1	11.2	8.2	−2.7
$CoFe_2O_4$	−341548	30.1	39.9	4.2	3.3
Co_2SiO_4	−346170	38.2	41.1	4.4	−3.6

3.3. Thermodynamic Parameters. In order to determine the stability of cobalt ferrite and cobalt silicate, the variation of the standard enthalpy of formation (ΔH^o), entropy (S^o), and molar heat capacity ($c_p{}^o$) and the decomposition temperature (T_D) were calculated. For calculations, room temperature (T_o = 25°C) was considered as reference. The thermodynamic data of various reactants and products is presented in the literature [35]. The thermodynamic parameters of the compounds formed during synthesis are listed in Table 2. c_p was calculated according to the following equation [35, 36]:

$$c_p{}^o = a + bT + cT^2, \tag{3}$$

where a, b, and c are the molar heat capacity coefficients characteristics of each substance and T is the temperature.

The standard enthalpy of formation at temperature T ($\Delta H_T{}^o$) was calculated using the values of standard enthalpy of formation at 25°C ($\Delta H_o{}^o$) (CoO = −60.5 kcal/mol, Fe_2O_3 = −44.4 kcal/mol, SiO_2 = −36.8 kcal/mol, $CoFe_2O_4$ = −541.7 kcal/mol, and Co_2SiO_4 = −55.2 kcal/mol) according to the following equation [35, 36]:

$$\Delta H_T{}^o = \Delta H_o{}^o + c_p{}^o \cdot (T\text{-}25)\,. \tag{4}$$

Using the values of the entropy at 25°C ($S_o{}^o$) (CoO = −53,5 cal/mol·K, Fe_2O_3 = −2588 cal/mol K, SiO_2 = −2497 cal/mol K, $CoFe_2O_4$ = −1461 cal/mol K, Co_2SiO_4 = −1495 cal/mol K), the entropy at temperature T ($S_T{}^o$) was calculated according to the following equation [36]:

$$S_T{}^o = S_o^o + \int_{25}^{T} c_p^o \frac{dT}{T}, \tag{5}$$

where S_o^o is the standard entropy at T = 25°C and c_p^o is the molar heat capacity.

The variation of Gibbs free energy ($\Delta G_T{}^o$) in function of the temperature in standard condition was calculated according to the following equation [36]:

$$\Delta G_T{}^o = \Delta H_T{}^o - T * S_T{}^o, \tag{6}$$

where $\Delta G_T{}^o$ is the variation of Gibbs free energy, ΔH^o is the enthalpy variation at temperature T, T is the temperature, and $\Delta S_T{}^o$ is the entropy at temperature T.

Table 3 presents the thermodynamic parameters calculated for CoO, Fe_2O_3, and SiO_2, while Table 4 presents the thermodynamic data calculated for olivine and cobalt ferrite.

Considering that the equilibrium between different reaction products $CoFe_2O_4$ and Co_2SiO_4 and their precursors (CoO, Fe_2O_3, and SiO_2) is influenced by the value of the thermodynamic parameters, the variation of these parameters was calculated. The decomposition of cobalt ferrite takes place according to (7).

$$CoFe_2O_4 \longrightarrow CoO + Fe_2O_3 \tag{7}$$

The calculations were performed using the thermal decomposition of oxalates (in case of using 1,2-EG as chelator) which corresponds to the temperature at which the pressure of CO_2 is equal to 1 atmosphere.

The thermodynamic data presented in Tables 3 and 4 was used to calculate the reaction enthalpy (ΔH_R) and reaction entropy (ΔS_R) for cobalt ferrite decomposition according to (8) and (9):

$$\Delta H_R = \sum n_{\text{prod}} \cdot \Delta H^0_{\text{prod}} - \sum n_{\text{react}} \cdot \Delta H^0_{\text{react}}, \tag{8}$$

where n_{prod} and n_{react} are the stoichiometric coefficients of reaction products and reactants, respectively, and ΔH^0_{prod} and $\Delta H^0_{\text{react}}$ are the variations of enthalpy of reaction products and reactants, respectively.

$$\Delta S_R = S_o^o + \int_{25}^{T} n_{\text{prod}} \cdot c^o_{p,\text{prod}} \frac{dT}{T} - \int_{25}^{T} n_{\text{react}} \cdot c^o_{p,\text{react}} \frac{dT}{T}, \tag{9}$$

where S_o^o is the standard entropy at T = 25°C, n_{prod} and n_{react} are the stoichiometric coefficients of reaction products and reactants, and $c^o_{p,\text{prod}}$ and $c^o_{p,\text{react}}$ are the molar heat capacities of reaction products and reactants, respectively.

The variation of Gibbs free energy of the reaction (ΔG_R) was calculated according to (6) using calculated ΔH_R and ΔS_R. In the case of cobalt ferrite decomposition, the reaction enthalpy and entropy increase with the increase of temperature and decrease with the decrease of free enthalpy (Figure 6). There is a temperature range where ΔG_R = 0 and ΔG_R can be calculated by interpolation using the function $\Delta G_R = f(T)$. The decomposition temperature is considered the temperature where ΔH_R = 0.

Table 5 shows the thermodynamic parameters at decomposition temperature (T_D = 348°C) for cobalt ferrite. The necessary enthalpy to reach the decomposition temperature is 642 kcal/mol. The decomposition temperature is reached when the lattice energy of the reaction products is equal to the lattice energy of cobalt ferrite. If the lattice energy of cobalt ferrite is lower, it tends to pass into a more stable form. In our case, the lattice energy of cobalt ferrite is lower than that of the two reaction products.

Table 3: Thermodynamic parameters at different temperatures for CoO, SiO_2, and Fe_2O_3.

T (°C)	$c_p{}^o$ (cal/mol·K)			ΔH^o (kcal/mol)			S^o (cal/mol·K)			ΔG^o (kcal/mol)		
	CoO	Fe_2O_3	SiO_2	CoO	Fe_2O_3	SiO_2	CoO	Fe_2O_3	SiO_2	CoO	Fe_2O_3	SiO_2
25	12.6	2560	2471	−57.1	−58.1	4.7	12.7	31.1	26.5	−60.9	−67.4	−3.2
100	12.6	3409	3291	−55.8	240	293	16.4	884	850	−62.4	−113	−47.1
200	12.7	4258	4111	−54.6	624	663	19.4	1736	1672	−64.1	−244	−173
300	12.9	5107	4931	−53.3	1092	115	21.5	2587	2494	−66.2	−460	−381
400	13.0	5956	5751	−52.0	1645	1649	23.5	3438	3316	−68.4	−761	−672
500	13.2	6805	6571	−50.7	2283	2265	25.3	4288	4137	−70.9	−1148	−1045
600	13.4	7654	7391	−49.3	3006	2963	26.8	5139	4959	−73.5	−1619	−1499
700	13.6	8503	8211	−48.0	3814	3744	28.3	5989	5780	−76.2	−2176	−2036
800	13.8	9352	9031	−46.6	4706	4606	29.6	6839	6601	−79.1	−2817	−2655
900	14.0	10201	9851	−45.2	5684	5550	30.8	7690	7422	−82.2	−3543	−3357

Table 4: Thermodynamic parameters at different temperatures for $CoFe_2O_4$ and Co_2SiO_4.

T (°C)	$c_p{}^o$ (cal/mol·K)		ΔH^o (kcal/mol)		S^o (cal/mol·K)		ΔG^o (kcal/mol)	
	$CoFe_2O_4$	Co_2SiO_4	$CoFe_2O_4$	Co_2SiO_4	$CoFe_2O_4$	Co_2SiO_4	$CoFe_2O_4$	Co_2SiO_4
25	1312	1348	−339	−343	38.8	47.2	−351	−358
100	1736	1785	−187	−187	474	495	−376	−385
200	2151	2221	8.24	13.5	907	940	−445	−457
300	2584	2657	245	257	1339	1384	−558	−573
400	3008	3093	525	545	1769	1826	−713	−733
500	3432	3529	847	876	2198	2268	−911	−938
600	3856	3965	1211	1251	2627	2708	−1153	−1187
700	4280	4401	1618	1669	3055	3149	−1437	−1480
800	4704	4837	2067	2131	3483	3589	−1764	−1816
900	5128	5273	2559	2636	3910	4028	−2133	−2197

Table 5: Thermodynamic parameters for cobalt ferrite decomposition at the decomposition temperature.

Compound	$c_p{}^o$ (cal/mol·K)	ΔH^o (kcal/mol)	S^o (cal/mol·K)	ΔG^o (kcal/mol)
$CoFe_2O_4$	2673	301	1429	−587
CoO	12.9	−53.0	21.9	−66.6
Fe_2O_3	5285	1201	2766	−517
T_D	2625	847	1359	3.5

Table 6: Thermodynamic parameters for olivine decomposition at the decomposition temperature.

Compound	$c_p{}^o$ (cal/mol·K)	ΔH^o (kcal/mol)	S^o (cal/mol·K)	ΔG^o (kcal/mol)
$CoFe_2O_4$	2848	378	1577	−638
CoO	12.9	−52.7	22.4	−67.1
Fe_2O_3	5290	1339	2854	−499
T_D	2468	855	1321	4.7

Similarly, the thermodynamic parameters were calculated for the reaction of olivine decomposition according to (10).

$$Co_2SiO_4 \longrightarrow 2CoO + SiO_2 \quad (10)$$

Also, in the case of olivine decomposition, the reaction enthalpy and entropy increase with increase of temperature and decrease with the decrease of free enthalpy (Figure 7). Table 6 shows the thermodynamic parameters at the

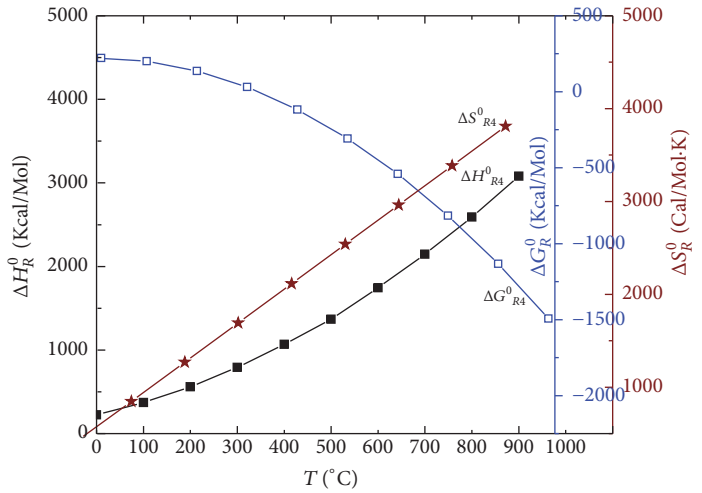

Figure 6: Variation of thermodynamic parameters for cobalt ferrite decomposition.

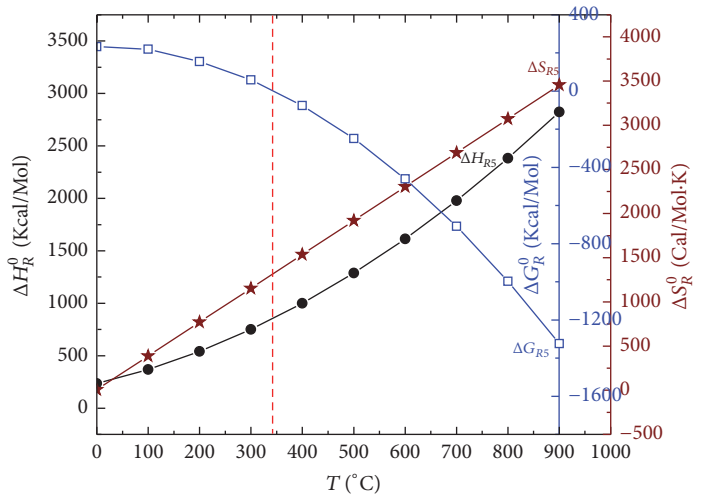

Figure 7: Variation of thermodynamic parameters for olivine decomposition.

decomposition temperature for olivine (T_D = 370.6°C). The necessary enthalpy to reach the decomposition temperature is 724 kcal/mol.

3.4. SEM and TEM Analysis. Figure 8 shows the SEM images of $CoFe_2O_4$ nanocrystallites embedded in the silica matrix. The SEM images revealed spherical particles assembled in high agglomerations of irregular shape.

Using 1,2-ED and 1,4-BD for the carboxylate precursor obtaining, larger agglomerates were observed. The agglomerates' size increases also with the annealing temperature.

The TEM images (Figure 9) show that the size of the nanoparticle spheres increases with the number of methylene groups of the carboxylate precursor. The size of nanocrystallites obtained from the Scherrer equation was confirmed by the nanoparticle size obtained from TEM images. In the case of gels annealed at 900°C, nanoparticles of 10 nm to 23 nm diameters were obtained.

4. Conclusions

The embedding of the reactants in the silica matrix followed by the redox reaction with formation of carboxylate type precursors (oxalate, malonate, and succinate, respectively) and their thermal decomposition allowed the obtaining of 70% $CoFe_2O_4$/30% SiO_2 (wt%) nanocomposites. Longer

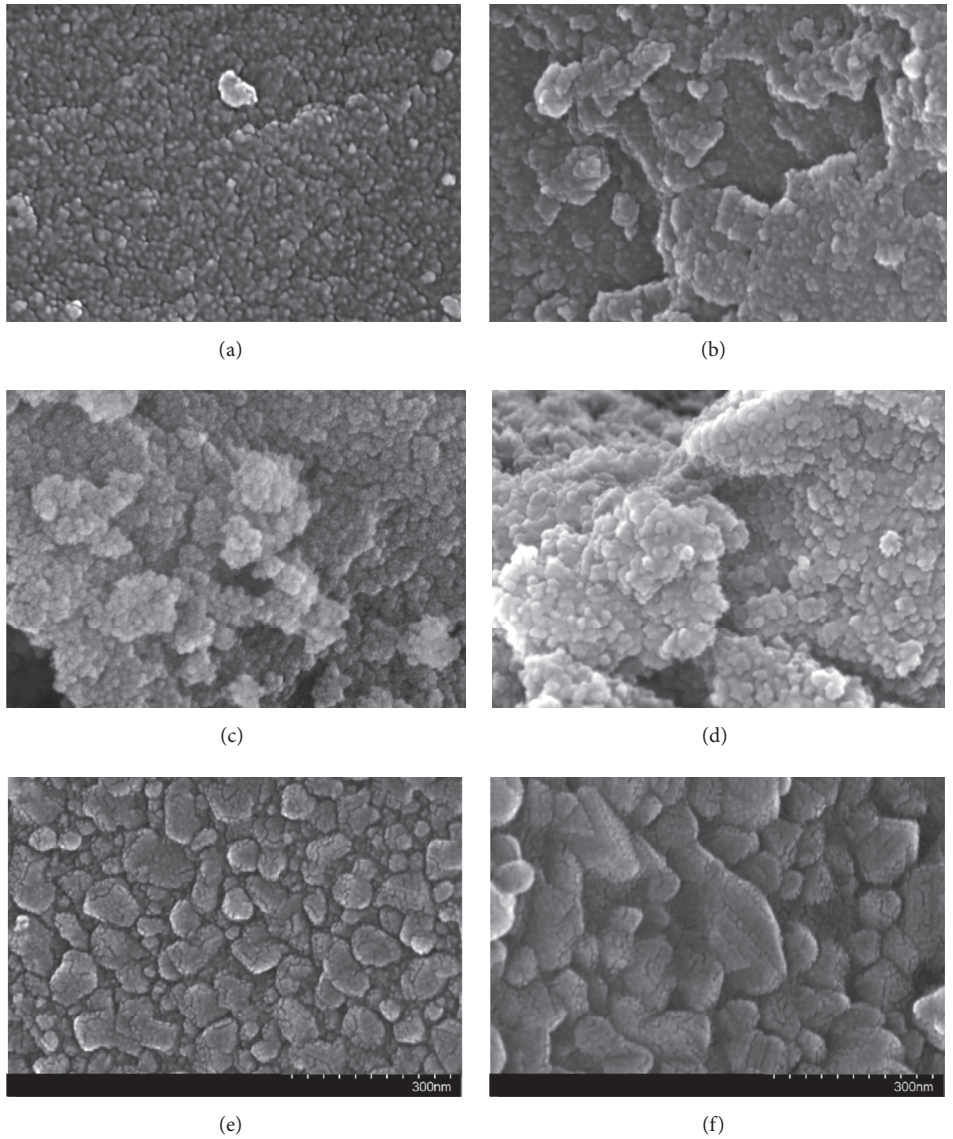

Figure 8: SEM images of gels obtained using 1,2-ED, 1,3-PD, and 1,4-BD, annealed at 700 and 900°C.

chain diols resulted in higher weight losses in the decomposition process of the precursors and higher decomposition temperature. Longer chain precursors embedded in the silica matrix favored the formation of single phase cobalt ferrite, at lower temperatures: Co and Fe succinates allow the obtaining of crystalline cobalt ferrite at 500°C, while Co and Fe oxalates give amorphous cobalt ferrite at 500°C, poorly crystalline cobalt ferrite with traces of olivine at 700°C, and single phase crystalline cobalt ferrite at 900°C. The average nanocrystallites size of cobalt ferrite ranges from 11 to 22 nm in case of annealing at 900°C, while in case of using 1,4-BD the average nanocrystallite size can reach 5 nm after annealing at 500°C. The nanocrystallites' size increases with the increase of the methylene groups in the precursors and the annealing temperature. The enthalpy and entropy of the cobalt ferrite and olivine decomposition reaction increase with the increase of annealing temperature. The presented synthesis method offers a viable alternative for obtaining $CoFe_2O_4/SiO_2$ nanocomposites with applications in the field of catalysis and magnetic materials.

Conflicts of Interest

The authors declare that there are no conflicts of interest regarding the publication of this paper.

Acknowledgments

The authors are grateful for financial support from the National Authority for Scientific Research and Innovation

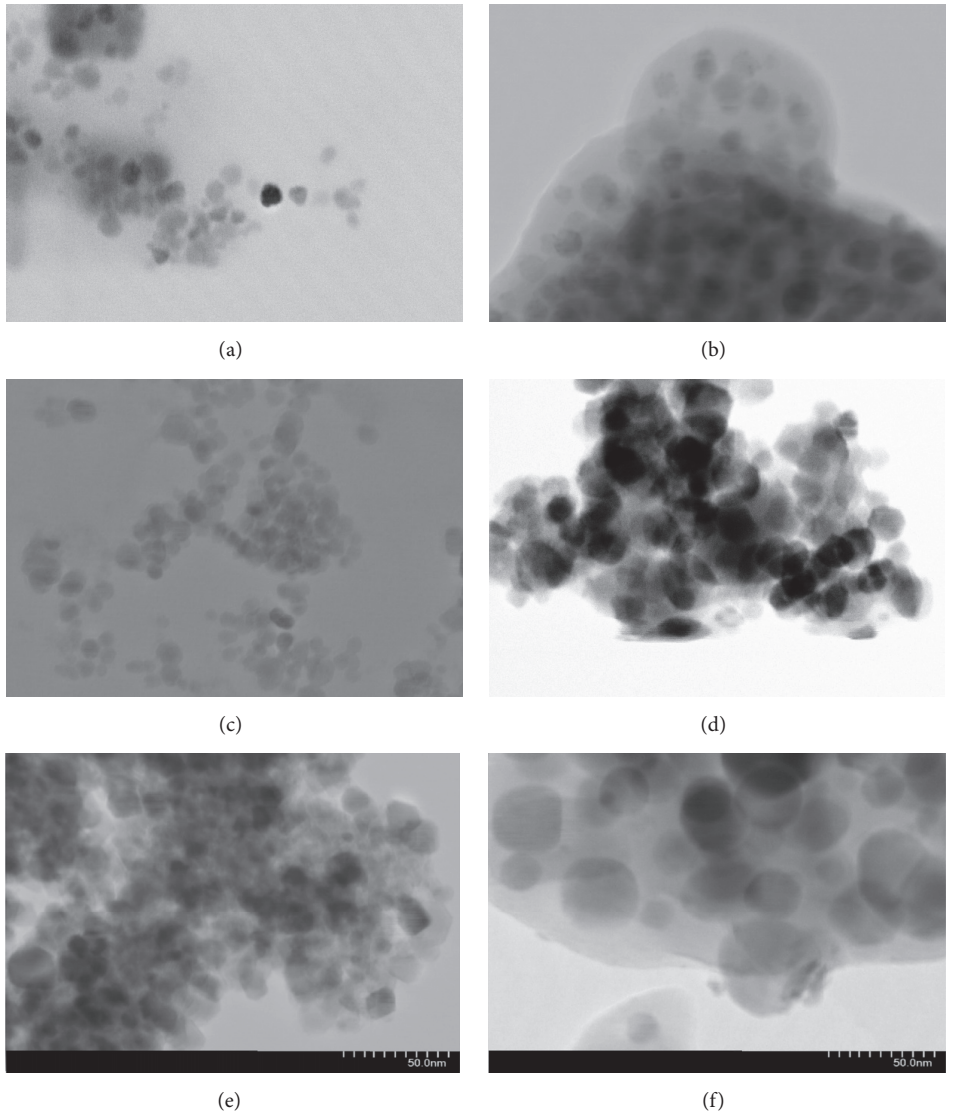

Figure 9: TEM images of gels obtained using 1,2-ED, 1,3-PD, and 1,4-BD, annealed at 700 and 900°C.

(ANCSI) Core Program (Project no. 16.40.02.01) and Sectoral Operational Programme "Increase of Economic Competitiveness", Priority Axis II (Project no. 1887, INOVAOPTIMA, code SMIS-CSNR 49164).

References

[1] P. H. C. Camargo, K. G. Satyanarayana, and F. Wypych, "Nanocomposites: synthesis, structure, properties and new application opportunities," *Materials Research*, vol. 12, no. 1, pp. 1–39, 2009.

[2] F. Liu, S. Laurent, A. Roch, L. Vander Elst, and R. N. Muller, "Size-controlled synthesis of $CoFe_2O_4$ nanoparticles potential contrast agent for MRI and investigation on their size-dependent magnetic properties," *Journal of Nanomaterials*, vol. 2013, Article ID 462540, 9 pages, 2013.

[3] H. Jin, Q. Chen, Z. Chen, Y. Hu, and J. Zhang, "Multi-LeapMotion sensor based demonstration for robotic refine tabletop object manipulation task," *CAAI Transactions on Intelligence Technology*, vol. 1, no. 1, pp. 104–113, 2016.

[4] H. Wei, D. Ding, X. Yan et al., "Tungsten trioxide/zinc tungstate bilayers: electrochromic behaviors, energy storage and electron transfer," *Electrochimica Acta*, vol. 132, pp. 58–66, 2014.

[5] S. W. da Silva, R. C. Pedroza, P. P. C. Sartoratto et al., "Raman spectroscopy of cobalt ferrite nanocomposite in silica matrix prepared by sol-gel method," *Journal of Non-Crystalline Solids*, vol. 352, no. 9-20, pp. 1602–1606, 2006.

[6] S. Wei, Q. Wang, J. Zhu, L. Sun, H. Lin, and Z. Guo, "Multifunctional composite core-shell nanoparticles," *Nanoscale*, vol. 3, no. 11, pp. 4474–4502, 2011.

[7] B. G. Toksha, S. E. Shirsath, S. M. Patange, and K. M. Jadhav, "Structural investigations and magnetic properties of cobalt ferrite nanoparticles prepared by sol-gel auto combustion

method," *Solid State Communications*, vol. 147, no. 11-12, pp. 479–483, 2008.

[8] T. Ramesh, S. Bharadwaj, and S. R. Murthy, "$CoFe_2O_4$-SiO_2 composites: preparation and magnetodielectric properties," *Journal of Materials*, vol. 2016, Article ID 7518468, 7 pages, 2016.

[9] C. H. Chia, S. Zakaria, M. Yusoff et al., "Size and crystallinity-dependent magnetic properties of $CoFe_2O_4$ nanocrystals," *Ceramics International*, vol. 36, no. 2, pp. 605–609, 2010.

[10] X.-M. Liu, S.-Y. Fu, and L.-P. Zhu, "High-yield synthesis and characterization of monodisperse sub-microsized $CoFe_2O_4$ octahedra," *Journal of Solid State Chemistry*, vol. 180, no. 2, pp. 461–466, 2007.

[11] M. M. El-Okr, M. A. Salem, M. S. Salim, R. M. El-Okr, M. Ashoush, and H. M. Talaat, "Synthesis of cobalt ferrite nano-particles and their magnetic characterization," *Journal of Magnetism and Magnetic Materials*, vol. 323, no. 7, pp. 920–926, 2011.

[12] M. Houshiar, F. Zebhi, Z. J. Razi, A. Alidoust, and Z. Askari, "Synthesis of cobalt ferrite ($CoFe_2O_4$) nanoparticles using combustion, coprecipitation, and precipitation methods: a comparison study of size, structural, and magnetic properties," *Journal of Magnetism and Magnetic Materials*, vol. 371, pp. 43–48, 2014.

[13] L. A. García Cerda and S. M. Montemayor, "Synthesis of $CoFe_2O_4$ nanoparticles embedded in a silica matrix by the citrate precursor technique," *Journal of Magnetism and Magnetic Materials*, vol. 294, no. 2, pp. e43–e46, 2005.

[14] F. Huixia, C. Baiyi, Z. Deyi, Z. Jianqiang, and T. Lin, "Preparation and characterization of the cobalt ferrite nano-particles by reverse coprecipitation," *Journal of Magnetism and Magnetic Materials*, vol. 356, pp. 68–72, 2014.

[15] D. Zhao, X. Wu, H. Guan, and E. Han, "Study on supercritical hydrothermal synthesis of $CoFe_2O_4$ nanoparticles," *Journal of Supercritical Fluids*, vol. 42, no. 2, pp. 226–233, 2007.

[16] Q. Lin, J. Lin, Y. He, R. Wang, and J. Dong, "The structural and magnetic properties of gadolinium doped $CoFe_2O_4$ nanoferrites," *Journal of Nanomaterials*, vol. 2015, Article ID 294239, 6 pages, 2015.

[17] S.-P. Rwei, L. Y. Wang, and P.-W. Yang, "Synthesis and magnetorheology study of iron oxide and iron cobalt oxide suspensions," *Journal of Nanomaterials*, vol. 2013, Article ID 612894, 7 pages, 2013.

[18] D. Gingasu, I. Mindru, L. Patron et al., "Green synthesis methods of $CoFe_2O_4$ and Ag-$CoFe_2O_4$ nanoparticles using hibiscus extracts and their antimicrobial potential," *Journal of Nanomaterials*, vol. 2016, Article ID 2106756, 12 pages, 2016.

[19] J. Chen, Y. Wang, and Y. Deng, "Highly ordered $CoFe_2O_4$ nanowires array prepared via a modified sol-gel templated approach and its optical and magnetic properties," *Journal of Alloys and Compounds*, vol. 552, no. 5, pp. 65–69, 2013.

[20] T. Dippong, O. Cadar, E. A. Levei et al., "Structure and magnetic properties of $CoFe_2O_4$/SiO_2 nanocomposites obtained by sol-gel and post annealing pathways," *Ceramics International*, vol. 43, no. 2, pp. 2113–2122, 2017.

[21] M. Shi, R. Zuo, Y. Xu et al., "Preparation and characterization of $CoFe_2O_4$ powders and films via the sol-gel method," *Journal of Alloys and Compounds*, vol. 512, no. 1, pp. 165–170, 2012.

[22] P. Barvinschi, O. Stefanescu, T. Dippong, S. Sorescu, and M. Stefanescu, "$CoFe_2O_4$/SiO_2 nanocomposites by thermal decomposition of some complex combinations embedded in hybrid silica gels," *Journal of Thermal Analysis and Calorimetry*, vol. 112, no. 1, pp. 447–453, 2013.

[23] M. Stefanescu, M. Stoia, T. Dippong, O. Stefanescu, and P. Barvinschi, "Preparation of $Co_xFe_{3-x}O_4$ oxydic system starting from metal nitrates and propanediol," *Acta Chimica Slovenica*, vol. 56, no. 2, pp. 379–385, 2009.

[24] T. Dippong, E. A. Levei, G. Borodi, F. Goga, and L. Barbu Tudoran, "Influence of Co/Fe ratio on the oxide phases in nanoparticles of $Co_xFe_{3-x}O_4$," *Journal of Thermal Analysis and Calorimetry*, vol. 119, no. 2, pp. 1001–1009, 2015.

[25] W. Pon-On, N. Charoenphandhu, I.-M. Tang, P. Jongwattanapisan, N. Krishnamra, and R. Hoonsawat, "Encapsulation of magnetic $CoFe_2O_4$ in SiO_2 nanocomposites using hydroxyapatite as templates: a drug delivery system," *Materials Chemistry and Physics*, vol. 131, no. 1-2, pp. 485–494, 2011.

[26] M. Kooti and E. Nasiri, "Phosphotungstic acid supported on silica-coated $CoFe_2O_4$ nanoparticles: an efficient and magnetically-recoverable catalyst for *N*-formylation of amines under solvent-free conditions," *Journal of Molecular Catalysis A: Chemical*, vol. 406, pp. 168–177, 2015.

[27] A. Pirouzfar and S. A. Seyyed Ebrahimi, "Optimization of sol-gel synthesis of $CoFe_2O_4$ nanowires using template assisted vacuum suction method," *Journal of Magnetism and Magnetic Materials*, vol. 370, pp. 1–5, 2014.

[28] X. Huang and Z. Chen, "Preparation of $CoFe_2O_4$/SiO_2 nanocomposites by sol-gel method," *Journal of Crystal Growth*, vol. 271, no. 1-2, pp. 287–293, 2004.

[29] X.-H. Huang and Z.-H. Chen, "Sol-gel preparation and characterization of $CoFe_2O_4$-SiO_2 nanocomposites," *Solid State Communications*, vol. 132, no. 12, pp. 845–850, 2004.

[30] A. Martucci, D. Buso, M. Guglielmi, L. Zbroniec, N. Koshizaki, and M. Post, "Optical gas sensing properties of silica film doped with cobalt oxide nanocrystals," *Journal of Sol-Gel Science and Technology*, vol. 32, no. 1–3, pp. 243–246, 2004.

[31] T. Dippong, E. A. Levei, O. Cadar, F. Goga, G. Borodi, and L. Barbu-Tudoran, "Thermal behavior of $Co_xFe_{3-x}O_4$/SiO_2 nanocomposites obtained by a modified sol–gel method," *Journal of Thermal Analysis and Calorimetry*, vol. 128, pp. 39–52, 2017.

[32] Y. Liu, C. Mi, L. Su, and X. Zhang, "Hydrothermal synthesis of Co_3O_4 microspheres as anode material for lithium-ion batteries," *Electrochimica Acta*, vol. 53, no. 5, pp. 2507–2513, 2008.

[33] T. Dippong, E. A. Levei, C. Tanaselia et al., "Magnetic properties evolution of the $Co_xFe_{3-x}O_4$/SiO_2 system due to advanced thermal treatment at 700◦c and 1000◦c," *Journal of Magnetism and Magnetic Materials*, vol. 410, pp. 47–54, 2016.

[34] H. P. Klug and L. E. Alexander, *X-Ray Diffraction Procedures*, John Wiley & Sons, New York, NY, USA, 2nd edition, 1974.

[35] I. Barin and O. Knacke, *Thermochemical Properties of Inorganic Substances*, Springer, Berlin, Germany, 1973.

[36] G. Bourcenu, "Fundamentele termodinamicii chimice," in *Fundamentele termodinamicii chimice*, A. I. Universitatii, Ed., Iasi, 1998.